

Analysis of the turn-off dynamics in polymer light-emitting diodes

D. J. Pinner, R. H. Friend, and N. Tessler^{a)}

Cavendish Laboratory, Madingley Road, Cambridge CB3 0HE, United Kingdom

(Received 21 July 1999; accepted for publication 29 December 1999)

We present experimental techniques to analyze the electroluminescence (EL) of polymer light-emitting diodes following the removal of an applied voltage pulse. We explain the fast modulation of the EL intensity at turn-off in terms of the sudden reduction of the Langevin recombination rate, and extract the time evolution the device's internal electric field at the recombination zone during the application of a voltage pulse. The results are compared to, and found to be consistent with, those of simple numerical modeling. The subsequent long-lived EL tail is analyzed to give the time evolution of the carrier distributions at the recombination zone once the voltage pulse has been removed. © 2000 American Institute of Physics. [S0003-6951(00)00109-1]

Excitation of polymer light-emitting diodes (LEDs) using electrical pulses has been used by several authors to study the processes leading to electroluminescence (EL).¹⁻¹⁰ In previous publications,^{6,10} we proposed a method which related the "turn-on" characteristics of the EL to the field-dependent mobility of holes and electrons. In this letter, we analyze the behavior of the EL after "turn-off" (i.e., once the voltage has been removed).

We describe two LED structures: device A [ITO/PEDOT:PSS (50 nm)/PPV copolymer (75 nm)/Ca], as was characterized in Ref. 6 in terms of EL turn-on, and device B [ITO/PPV (220 nm)/Ag]. PEDOT:PSS stands for doped polyethylene dioxythiophene/polystyrene sulphonate (Refs. 11 and 12) and PPV for poly(*p*-phenylenevinylene). Further experimental details may be found in Refs. 6 and 9.

The behavior of the LED after turn-off is dependent on the density distributions of electrons and holes (n and p , respectively), and on the internal electric field F_{int} remaining inside the device. In a previous publication,^{6,10} we presented details of a numerical model used to simulate the transient response of LEDs to voltage pulses. Figure 1 shows the numerically simulated internal electric field for several different times, as a function of distance from the cathode z for a device of thickness $l = 100$ nm in response to $10 \mu\text{s}$ pulses of applied voltage $V_{\text{app}} = 7$ V. The inset of Fig. 1 shows the calculated transient EL intensity. Before the pulse application ($t < 0$), the electric field in the bulk of the polymer is largely determined by the built-in field $F_{\text{bi}} = V_{\text{bi}}/l$, where V_{bi} is the built-in voltage [~ -1.9 V for device A (Ref. 10)]. Upon application of the voltage pulse at $t = 0$, the polymer-electrode interfaces become charged within the RC time of the experimental setup (here, $RC \sim 1-10$ ns). Significant injection of charge into the bulk of the device, however, does not commence until flatband conditions have been achieved within the device, i.e., until $V_{\text{LED}} + V_{\text{bi}} = 0$, where V_{LED} is the voltage at the LED. Assuming a simple series R and C circuit, the time taken to achieve the flatband condition, $t = t(-V_{\text{bi}})$, is given by

$$t(-V_{\text{bi}}) = RC \ln\{V_{\text{app}}/(V_{\text{bi}})\}, \quad (1)$$

from which we calculated $t(-V_{\text{bi}}) \sim 0.7, 0.2,$ and $0.05RC$ for $V_{\text{app}} = 4, 10,$ and 40 V, respectively. We, therefore, conclude that the charging of the device includes charge injection into the bulk of the LED.

Once injection begins, the hole carrier packet propagates towards a quasistationary sheet of electrons at the cathode [in most organic materials ($\mu_e \ll \mu_h$) (Ref. 6)]. EL turn-on occurs at time $t = t_d$ (see Fig. 1 inset) when the leading edge of the hole packet reaches the electrons confined close to the cathode. The EL then rises rapidly for a further time t_1 (see Fig. 1 inset) as the main body of the hole packet arrives at the cathode. See Ref. 6 for details of the methodology used to determine t_d and t_1 . On a longer time scale, electrons propagate into the device, resulting in a slower rise in the EL.

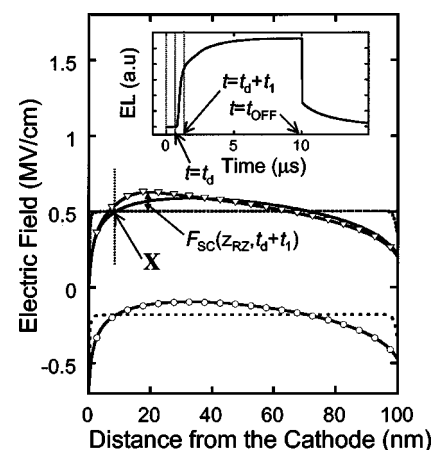


FIG. 1. Calculated electric-field distribution for five different points in time: (1) $t < 0$ (dashed line), before the applied pulse; (2) $t = 0$ (dotted line) just after the applied pulse and before the buildup of space charge; (3) $t = t_d + t_1$ (open upside-down triangles) once the holes have propagated through the structure; (4) $t = t_{\text{SS}}$ (unbroken line) at quasisteady state where space charge is due to both electrons and holes; and (5) $t = t_{\text{OFF}} + 1$ ns (open circles) just after voltage is turned off. The inset shows the simulated response of the EL intensity for a PPV-like device (similar to device A) to a square voltage pulse ($V_{\text{app}} = 7$ V, $w = 10 \mu\text{s}$). The assumptions used for this simulation can be found in Ref. 6.

^{a)}Current address: EE Dept. Technion, Haifa 32000, Israel; electronic mail: nir@ee.technion.ac.il

The space charge that builds up throughout the charge injection process induces an electric-field distribution $F_{SC}(z)$ such that $F_{int}(z) = F_{app} + F_{bi} + F_{SC}(z)$, where $F_{app} = V_{app}/l$, $F_{bi} = V_{bi}/l$, and $F_{int}(z)$ is the total internal electric field. We see from $F_{int}(z)$ at $t = t_d + t_1$ (Fig. 1) that the space charge reduces the electric field near the contacts and increase the electric field in the bulk of the device. The recombination zone was found to be located approximately at the position of the electric-field maximum,⁶ i.e., close to the cathode. The EL for $t > t_d + t_1$ is dominated by the slower migration of the electron packet into the device until the electron's density distribution reaches steady state at $t = t_{SS}$. The maximum in $F_{int}(z)$ at $t = t_{SS}$, having both moved further away from the cathode and reduced in magnitude, shows how the additional electrons further screen the electric field close to the cathode.

Upon removal of the applied voltage at $t = t_{OFF}$, both experiment⁶ and simulation (inset of Fig. 1) show that the EL undergoes a fast modulation to a small but nonzero value, followed by a long-lived EL tail. To analyze this further, we write down the expression for L_T , the total Langevin excitation generation in the device,

$$L_T = A \int_0^l L(z) dz = A \int_0^l B \mu_{eff}(z) n(z) p(z) dz, \quad (2)$$

where A is the area of the LED, $L(z)$ is the Langevin excitation generation rate per unit volume at distance z from the cathode, B is a constant, and μ_{eff} is the effective mobility of the electrons and holes. Since numerical simulations^{6,10} of device A show that the spatial extent of the recombination zone Δz_{RZ} , is very small with respect to l , L_T in Eq. (2) may be approximated to $L(z_{RZ}) \Delta z_{RZ} A$, where $z = z_{RZ}$ is the position of the center of the recombination zone. The large mismatch between the hole and electron mobilities also implies that $\mu_{eff} \sim \mu_h$, where μ_h is field dependent through the equation¹³

$$\mu_h(z) = \mu_{h,0} \exp\left(-\frac{\Delta}{kT}\right) \exp(\gamma |\sqrt{F_{int}(z)}|), \quad (3)$$

where $\mu_{h,0}$ is a constant, Δ is the activation energy, k is the Boltzmann constant, T is the temperature, $\gamma = b(1/kT - 1/kT_0)$, and b and T_0 are material constants. For the ITO/PEDOT/PPV copolymer/Ca device used in this work, we previously measured⁶ $\gamma = 1.0 \times 10^{-2} \text{ (cm/V)}^{1/2}$ at room temperature.

The fast EL modulation has previously been shown¹⁰ to result from the instantaneous reduction of the internal field from $F_{int}(z) = F_{app} + F_{bi} + F_{SC}(z)$ to $F_{int}(z) = F_{bi} + F_{SC}(z)$ at $t = t_{OFF}$ and, therefore, also to the Langevin recombination rate (and EL). Computer simulations^{6,10} indicate that the time for this EL modulation is determined by the singlet decay time (~ 1 ns), after which time the carrier density distributions n and p are effectively unchanged, as was experimentally verified in Ref. 10. Combining this point with Eqs. (2) and (3), the ratio of the EL immediately before and after turn-off is given by

$$\frac{EL(t'=0)}{EL(t' \cong 1 \text{ ns})} = \frac{\exp(\gamma (|F_{app} + F_{SC}(z_{RZ}) + F_{bi}|)^{1/2})}{\exp(\gamma (|F_{SC}(z_{RZ}) + F_{bi}|)^{1/2})}, \quad (4)$$

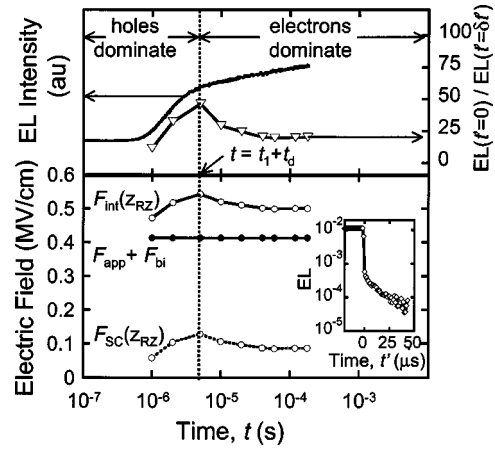


FIG. 2. Plot of the internal and space-charge-induced electric fields as a function of pulse application time t calculated for device A from the ratio of the EL before and immediately after voltage turn-off. Also shown is the transient EL of device A in response to a 5 V step voltage showing how the maximum in the calculated space-charge-induced field coincides with the time at which there exists the greatest imbalance between the number of holes and electrons in the device. The inset shows the EL (on a logarithmic scale) after the removal of a 5 V 200 μ s pulse.

where $t' = t - t_{OFF}$. Equation (4) can be used to calculate $F_{SC}(z_{RZ})$, the value of the space-charge-induced electric field at the position of the recombination zone. By doing this for pulses of different widths, we may determine the time evolution of the space-charge-induced electric field at the position of the recombination zone as a function of time *during* the applied pulse. The inset of Fig. 2 shows the EL response at turn-off for device A in response to 200 μ s 5 V pulses as a function of t' . The value of EL ($t' = \delta t'$) is taken as the point of inflexion on the downward slope of the EL after $t' = 0$. (Note that in practice $\delta t' > 1$ ns due to the resolution of the system). Figure 2 shows the ratio $EL(t' \cong \delta t')/EL(t' = 0)$ and the calculated values of $F_{SC}(z_{RZ}, t)$, $F_{app} + F_{bi}$, and $F_{int}(z_{RZ}, t)$ as a function of time t (not t'). Also shown is the measured EL response of device A to a 5 V step voltage to illustrate the correlation between the calculated electric fields and the measured EL. At this relatively low applied bias $F_{SC}(z_{RZ})$ is found to be in the same direction as the applied field (as predicted in Fig. 1) and it rises from 0 MV/cm at $t = 0$ to a maximum value of ~ 0.13 MV/cm at $t \sim t_d + t_1$ ($\sim 5 \mu$ s), after which it decreases to attain a steady-state value of ~ 0.09 MV/cm. This behavior is consistent with the simulation model, which shows that the peak value of the electric field reaches a maximum value at $t = t_d + t_1$ before attaining a steady-state value [see $F_{SC}(z_{RZ})$ in Fig. 1]. Comparing this with the measured EL, we see that the maximum in $F_{SC}(z_{RZ})$ occurs as the EL response changes from being dominated by hole to electron transport, i.e., the time at which there is the greatest difference between the densities of holes and electrons in the device. For $t > t_d + t_1$, the additionally injected electrons then reduce the value of $F_{SC}(z_{RZ})$.

The amount of space charge in the device may also be controlled by applying pulses of identical widths but different voltages. Figure 3 shows the turn-off behavior of the EL of device B (ITO/PPV/Ag) to 700 ns pulses of applied voltages 30, 35, and 40 V. The inset of Fig. 3 shows both the values of $F_{SC}(z_{RZ})$ [calculated using $\gamma = 6 \times 10^{-3}$ AIP license or copyright, see <http://jps.aip.org/aplo/aplcr.jsp>

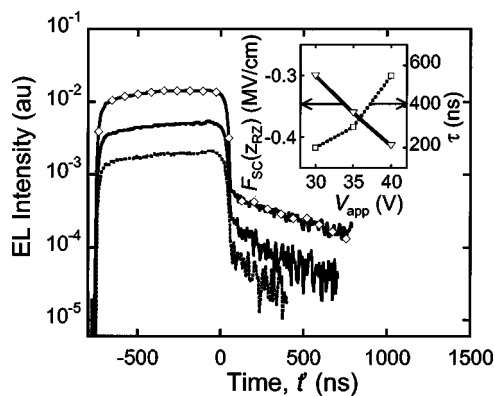


FIG. 3. EL intensity on a logarithmic scale for device B in response to 700 ns pulses of 30 V (dotted line), 35 V (unbroken line), and 40 V (open diamonds). $t' = 0$ corresponds to the time at which the voltage pulse was removed. The inset shows the space-charge-induced electric field at the position of the recombination zone immediately after turn-off calculated from the transient data, as a function of the applied voltage. Also shown is the time constant τ associated with the EL (and charge distribution) decay.

(cm/V)^{1/2}] (Ref. 13) and the time constant τ associated with the subsequent EL decay as a function of V_{app} . We see that $F_{SC}(z_{RZ})$ is increasingly negative at higher voltages, and that by extrapolating back to lower voltages, $F_{SC}(z_{RZ})$ is likely to flip sign from positive to negative at some lower applied voltage. This may be understood by referring back to the electric-field profiles in Fig. 1, from which we see that $F_{SC}(z)$ is negative near the electrodes and positive in the bulk of the device, i.e., the sign of $F_{SC}(z_{RZ})$ is determined by the position of the recombination zone relative to point X.

The long-lived EL tail following the fast modulation (seen in Figs. 2 and 3) is due to excitons generated from the decaying carrier densities in the presence of both F_{bi} and $F_{SC}(z_{RZ})$. Numerical simulations indicate, however, that $F_{SC}(z_{RZ})$ does not change considerably in comparison to the carrier densities. This is supported by the experimental observation that the long-time (up to ms) decay of the EL and the charges are very similar.¹⁰ In this case, we may use the long-lived EL decay to monitor the evolution of the carrier density distributions, rather than the electric field, after voltage turn-off.

From Fig. 3 we see that following the fast EL modulation at turn-off, the EL tail is well fitted to a single exponential of time constant τ . The fact that τ increases with V_{app} (see Fig. 3 inset) may be attributable to the additional Cou-

lombic attraction between holes and electrons due to the greater electron densities present at higher voltages. In other words, the residence time of the charges seems not to be due to extrinsic traps in the polymer but rather to the low mobility, at low fields, and the Coulomb attraction between oppositely charged carriers.

In summary, we have presented methods of investigating the carrier dynamics in polymer LEDs after the removal of an electrical pulse, the results of which are in agreement with our numerical model.^{6,10} We have shown how the fast modulation of the EL may be analyzed to time resolve the space-charge-induced electric field at the position of the recombination zone. This method may be contrasted with electroabsorption techniques, which yield average values of the electric field, and which are hard to interpret in the presence of charges. We have also shown how the long-lived EL tail can be used to monitor the carrier density distributions as a function of time after turn-off.

The authors thank the George and Lillian Schiff Foundation and the Engineering and Physical Sciences Research Council for financial support, and Cambridge Display Technology for supplying the polymers. This work has been supported by the European Commission under Brite Euram Contract No. BRPR-CT97-0469 (OSCA).

- ¹P. W. M. Blom and M. C. J. M. Vissenberg, *Phys. Rev. Lett.* **80**, 3819 (1998).
- ²D. Braun, D. Moses, C. Zhang, and A. J. Heeger, *Appl. Phys. Lett.* **61**, 3092 (1992).
- ³I. H. Campbell, D. L. Smith, C. J. Neef, and J. P. Ferraris, *Appl. Phys. Lett.* **74**, 2809 (1999).
- ⁴S. Karg, V. Dyakonov, M. Meier, W. Riess, and G. Paasch, *Synth. Met.* **67**, 165 (1994).
- ⁵V. R. Nikitenko, Y. H. Tak, and H. Bäsler, *J. Appl. Phys.* **84**, 2334 (1998).
- ⁶D. J. Pinner, R. H. Friend, and N. Tessler, *J. Appl. Phys.* **86**, 5116 (1999).
- ⁷V. Savvateev, A. Yakimov, and D. Davidov, *Adv. Mater.* **11**, 519 (1999).
- ⁸N. Tessler, N. T. Harrison, D. S. Thomas, and R. H. Friend, *Appl. Phys. Lett.* **73**, 732 (1998).
- ⁹N. Tessler, N. T. Harrison, and F. R. H., *Adv. Mater.* **10**, 64 (1998).
- ¹⁰N. Tessler, D. J. Pinner, V. Cleave, D. S. Thomas, G. Yahiolglu, P. Lebarney, and R. H. Friend, *Appl. Phys. Lett.* **74**, 2764 (1999).
- ¹¹S. A. Carter, M. Angelopoulos, S. Karg, P. J. Brock, and J. C. Scott, *Appl. Phys. Lett.* **70**, 2067 (1997).
- ¹²J. C. Carter, I. Grizzi, S. K. Heeks, D. J. Lacey, S. G. Latham, P. G. May, O. R. Delospanos, K. Pichler, C. R. Towns, and H. F. Wittmann, *Appl. Phys. Lett.* **71**, 34 (1997).
- ¹³P. W. M. Blom and M. J. M. de Jong, *IEEE J. Sel. Top. Quantum Electron.* **4**, 105 (1998).